Characterising Sediment Thickness beneath a Greenlandic Outlet Glacier using Distributed Acoustic Sensing: Preliminary Observations and Progress Towards an Efficient Machine Learning Approach

Adam D. Booth, Poul Christoffersen, Andrew Pretorius, Joseph Chapman, Bryn Hubbard, Emma C. Smith, Sjoerd de Ridder, Andy Nowacki, Bradley Paul Lipovsky, Marine Denolle

Abstract

Distributed Acoustic Sensing (DAS) is increasingly recognised as a valuable tool for glaciological seismic applications, although analysing the large data volumes generated in acquisitions poses computational challenges. We show the potential of active-source DAS to image and characterise subglacial sediment beneath a fast-flowing Greenlandic outlet glacier, estimating the thickness of sediment layers to be 20-30 m. However, the lack of subglacial velocity constraint limits the accuracy of this estimate. Constraint could be provided by analysing cryoseismic events in a counterpart 3-day record of passive seismicity, via (e.g.) seismic tomography, but locating them within the 9 TB data volume is computationally inefficient. We describe experiments with data compression using the frequency-wavenumber (f-k) transform ahead of training a convolutional neural network, that provides a ~300-fold improvement in efficiency. In combining active and passive-source and our machine learning framework, the potential of large DAS datasets could be unlocked for a range of future applications.

Introduction

Seismic methods are widely used to explore the internal and basal properties of glaciers and ice sheets (Podolskiy and Walter, 2016). Although seismic phenomena can be recorded at high temporal resolution, the spatial resolution of passive seismic data is often limited by the sparsity of seismometer arrays. This is partly addressed by the use of nodal seismic technologies (Karplus and others, 2021), but the recent development of Distributed Acoustic Sensing (DAS) offers the potential for metre-scale sampling along profiles that are many kilometres in length. The principle of DAS is reported elsewhere (Hartog, 2017; Lindsey and Martin, 2021) and it is sufficient here to understand that DAS effectively converts a length of fibre-optic cable into a continuous string of pseudo-seismometers (Zhu and others, 2021). DAS allows seismic vibrations to be recorded wherever fibre-optic cable can be deployed and coupled sufficiently well to the ground. Glaciological deployments of DAS include examples in the European Alps (Walter and others, 2020), Antarctica (Brisbourne and others, 2021; Hudson and others, 2021), Greenland (Booth and others, 2020) and Iceland (Fichtner and others, 2022), for both controlled-source and passive seismic applications.

Borehole DAS can be particularly valuable since fibre-optic cable is installed more simply and inexpensively than the same number of conventional seismic sensors for equal sample density. Booth and others (2020) reported the first glaciological deployment of borehole DAS, at RESPONDER project site S30 (70.56793°N, 50.08697°W) on *Sermeq Kujalleq* (Store Glacier), a major marine-terminating outlet of the Greenland Ice Sheet (Figure 1a). Fibre-optic cable was installed in a 1043 m-long vertical borehole drilled to the glacier bed. A Silixa iDAS™ system was used to acquire active-source vertical seismic profiles (VSPs) at various offsets and azimuths around the borehole, and a 3-day record of passive seismicity.

The vertical borehole geometry allows englacial and subglacial seismic structure to be determined more robustly than from surface seismic deployments, and thus improves the characterisation of physical properties including englacial water and ice fabric. Booth and others (2020) used active-source VSPs to determine a high-resolution depth profile of compressional (P-) wave velocity (Figure 1b), detecting the transition from isotropic to anisotropic ice at 84% of Store Glacier's thickness. Basal temperate ice was detected in the lowermost 100 m, confirmed separately by distributed temperature sensing in the same cable (Law and others, 2021). Reflections in the VSPs (Figure 2a) were observed but did not originate from the glacier bed, generated instead at a deeper horizon interpreted as the base of subglacial sediment. The time lag between a pair of direct and reflected waves implied a sediment thickness of 20 [-2, +17] m, assuming a sediment velocity of 1873 [-94, +1618] m s^{-1} (Hofstede and others, 2018).

The same approach was applied to the full suite of reflections in the active-source VSPs, allowing sediment thickness estimates to be mapped around the borehole up to radial distances of 200 m. This is possible because reflected energy measured at shallower borehole depth must reflect from a subsurface point at greater lateral offset (Figure 2b). Direct and reflected rays were traced through a 1-D velocity model, with deviations indicating a change in sediment thickness and/or velocity. Having no additional velocity constraint, we attributed all deviations to a thickness change, but our interpretation also neglects anisotropy and any local change in glacier thickness. Under these assumptions, preliminary estimates show sediment thickness varies between 20-30 m, with thinner sediment typically observed north of the borehole (Figure 2c).

Although the active-source shots provide rich azimuthal coverage, the velocity through the subglacial sediment remains unconstrained. The necessary constraint is potentially available, subject to location uncertainties, through analysis of subglacial cryoseismicity in the passive DAS record, via (e.g.) travel-time tomography (Zhang and others, 2020) but this is challenging given the volume of the recorded dataset: although only 3 days long, the record features 1043 seismic channels sampled at 4000 Hz and thus exceeds 9 TB in size. We are therefore exploring the implementation of convolutional neural networks (CNN) to efficiently identify and isolate cryoseismic events in the passive dataset, partly to complement active-source velocity analysis but also to elucidate the focal mechanism of seismic emissions.

Developing an Efficient CNN for recognising Cryoseismic Events

The complete architecture and performance of our CNN will be reported in a forthcoming publication, and the following summary is intended to provide sufficient information to appreciate preliminary results. The CNN was trained with an Adam optimizer (Kingma and Ba, 2015), using 36680 data windows of 0.25 s duration labelled as to whether they did (18360 windows, ~50%), or did not (18320 windows, ~50%), contain a cryoseismic arrival. Figure 3a shows an example of a prominent cryoseismic event, labelled (i), interpreted as arising from a crevassing event originating ~300 m deep in the glacier (consistent with crevasse observations at this depth in optical televiewer images; Hubbard and others, 2021). The arrivals at (i) are interpreted as the shear- (S-) wave component of the seismic wavefield; they are preceded, by ~0.1 s, by (ii) low-amplitude arrivals interpreted as the P-wave component. With velocities of 1800 m s^{-1} and 3750 m s^{-1} fit to the S- and P-wave components, the 0.1 s lag between them implies that crevassing occurs at a radial distance of ~350 m from the borehole. S-wave reflections from the glacier surface are observed at (iii).

29344 such windows were initially used to train the CNN, with 7336 for validation. Training took 100 epochs and was run on a standard specification laptop, but proved to be computationally inefficient: 129 s was required for the CNN to process 30 s of passive data, representing just 0.01% of the full data volume. We therefore explored an approach of training the CNN on data windows transformed into the frequency-wavenumber (f-k) domain. To the best of our knowledge, this strategy has not been explored before, likely because passive seismic arrays conventionally lack the high density of spatial samples of the DAS cable to make the f-k transformation worthwhile. On making this conversion (e.g., Figure 3b), the information contained in time domain windows is expressed using fewer data samples: the shape information in the time domain is preserved in the spread of apparent velocities in the f-k image, yet frequencies and wavenumbers outside of the range 0-150

Hz and ±0.4 m^{-1}, respectively, are redundant. When transformed to the f-k domain, the data volume in each 0.25 s window is reduced by a factor of ~350, and the analysis of 30 s data windows takes just 1.2 s (plus an additional 5.6 s to implement the transform). The success of the CNN is currently being assessed with a validation dataset that incorporates englacial, basal and subglacial seismicity and their different f-k expressions. We obtain an accuracy of 98% when testing with this validation dataset. CNN performance in the f-k domain is therefore considered promising both from accuracy and efficiency standpoints. Although more sophisticated machine learning approaches may be available (e.g., the residual neural network described by Dumont and others, 2020), we consider that the capabilities of our CNN may be sufficient for reliable event identification.

Outlook

Interest is growing in DAS deployments, but these need to happen alongside methodological developments to make data analysis practical. Our efficient compression of the passive seismic wavefield with frequency-wavenumber transforms makes analysis of the dataset tractable on standard CPUs, rather than GPUs or with specialist accelerators. The implementation of such algorithms could be vital for real-time monitoring of passive DAS deployments, allowing efficient recognition of crysoseismic events to trigger storage and/or transmission of data from a remote monitoring station.

Further development of such tools can benefit passive DAS applications for many glaciological studies. In addition to constraining subglacial velocities, integrated passive DAS and synchronous 3-component seismometer records allows the focal mechanism of cryoseismicity to be determined, thus improving our understanding of glacier dynamics. DAS data are also amenable to ambient noise cross-correlation, and recent results (Tribaldos and Ajo-Franklin, 2021) highlight how variations in seismic velocity are linked to changes in thermoelastic strain and hydrological dynamics.

Acknowledgments

Data acquisition was funded by the European Research Council as part of the RESPONDER project under the European Union's Horizon 2020 research and innovation program (Grant 683043). AB and BL were supported by Royal Society International Exchanges 2019 Round 3 funding, IES/R3/193115. BH was supported by a HERCW/Aberystwyth University Capital Equipment Grant. AP and ECS are funded by the NERC/NSF International Thwaites Glacier Collaboration *TIME* project (NE/S00677X/1). AN is funded by NERC project *Mantle Convection Constrained* (*MC*^{2}; NE/T012684/1). Silixa is thanked for supporting the DAS acquisition. We thank editor Francisco Navarro, Fabian Walter and an anonymous reviewer for constructive comments on this manuscript.

References

Booth AD, Christoffersen P, Schoonman C, Clarke A, Hubbard B, Law R, Doyle SH, Chudley TR and Chalari A (2020). Distributed Acoustic Sensing on a Fast-Flowing Greenlandic Outlet Glacier. Geophysical Research Letters, 47(13), e2020GL088148. 10.1029/2020GL088148.

Brisbourne A, Kendall M, Kufner SK, Hodson TS and Smith AM (2021). Downhole distributed acoustic sensing at Skytrain Ice Rise, West Antarctica. The Cryosphere, 15, 3443-3458. 10.1594/tc-15-3443/2021.

Dumont V, Tribaldos VR, Ajo-Franklin J and Wu K (2020). Deep learning for surface wave identification in distributed acoustic sensing data. In: 2020 IEEE International Conference on Big Data, 1293-1300. 10.1109/BigData50022.2020.9378084.

Fichtner A, Klaasen S, Thrastarson S, Çubuk-Sabuncu Y, Paitz P and Jónsdóttir K (2022). Fiber-Optic Observation of Volcanic Tremor through Floating Ice Sheet Resonance. The Seismic Record, 2(3), 148-155. 10.1785/03200220010.

Hartog, AH (2017). An introduction to distributed optical fibre sensors. Boca Raton, Florida: CRC Press/Taylor and Frances. 10.1201/9781315119014.

Hofstede C, Christoffersen P, Hubbard B, Doyle SH, Young TJ, Diez A, Eisen O and Hubbard A (2018). Physical Conditions of Fast Glacier Flow: 2. Variable Extent of Anisotropic Ice and Soft Basal Sediment form Seismic Reflection Data Acquired on Store Glacier, Greenland. Journal of Geophysical Research: Earth Surface, 123, 349-362. 10.1002/2017JF004297.

Hubbard B, Christoffersen P, Doyle SH, Chudley TR, Schoonman CM, Law R and Bougamont M (2021). Borehole-based characterization of deep mixed-mode crevasses at a Greenlandic outlet glacier. AGU Advances, 2, e2020AV00291. 10.1029/2020AV00291.

Hudson TS, Baird AF, Kendall JM, Kufner SK, Brisbourne AM, Smith AM, Butcher A, Chalari A and Clarke A (2021). Distributed Acoustic Sensing (DAS) for Natural Seismicity Studies: A Case Study from Antarctica. Journal of Geophysical Research: Solid Earth. 10.1029/2020JB021493.

Karplus M, Walter J and Tulaczyk S (2021). Thwaites Interdisciplinary Margin Evolution (TIME) Small Node Network. Dataset. International Federation of Digital Seismograph Networks. 10.7914/SN/1H_2021.

Kingma DP and Ba J (2015). Adam: A method for stochastic optimisation. 3rd International Conference for Learning Representations, San Diego, 2015. arXiv:1412.6908. 10.48550/arXiv.1412.6980.

Law R, Christoffersen P, Hubbard B, Doyle SH, Chudley TR, Schoonman CM, Bougamont M, Des Tombe B, Scihlperoort B, Kechavarzi C, Booth A and Young TJ (2021). Thermodynamics of a fast-moving Greenland outlet glacier revealed by fibre-optic distributed temperature sensing. Science Advances, 7(20), eabe7136. 10.1126/sciadv.abe7136.

Lindsey NJ and Martin ER (2021). Fibre-Optic Seismology. Annual Review of Earth and Planetary Sciences, 49, 309-336. 10.1146/annurev-earth-072420-065213.

Podolskiy EA and Walter F(2016). Cryoseismology. Reviews of Geophysics, 54(4), 708-758. 10.1002/2016RG000526.

Tribaldos VR and Ajo-Franklin JB (2021). Aquifer Monitoring using Ambient Seismic Noise recorded with DAS Deployed on Dark Fiber. Journal of Geophysical Research: Solid Earth, 126, e202JB021004. 10.1029./2020JB021004.

Walter F, Gräff D, Lindner F, Paitz P, Köpfil M, Chmiel M and Fichtner A (2020). Distributed acoustic sensing of microseismic sources and wave propagation in glaciated terrain. Nature Communications, 11, 2436. 10.1038/s41467-020-15824-6.

Zhang X, Roy C, Curtis A, Nowacki A and Baptie B (2020). Imaging the subsurface using induced seismicity and ambient noise: 3-D tomographic Monte Carlo joint inversion of earthquake body wave traveltimes and surface wave dispersion. Geophysical Journal International, 222(3), 1639-1655. 10.1093/gji/ggaa230.

Zhu T, Shen J and Martin ER (2021). Sensing Earth and environment dynamics by telecommunication fiber-optic sensors: an urban experiment in Pennsylvania, USA. Solid Earth, 12, 219-235. 10.5194/se-12-219-201.

FIGURE CAPTIONS

Figure 1. a) Site S30 on Store Glacier. Active-source shots (stars) are at various offsets and azimuths around a DAS-instrumented borehole. The offset VSP shown in Figure 2a uses the highlighted shotpoint. Inset panel: location in West Greenland. b) Vertical P-wave velocity trend, derived from zero-offset VSP data (Booth and others, 2020).

Figure 2. a) VSP record highlighting direct and reflected waves, and the lag time between them. b) Schematic VSP ray diagram for direct raypaths (blue) and subglacial reflections (red) from the base of a 30 m thick sediment layer. The lateral offset of the reflection point from the borehole increases the shallower the reflections are observed. c) Subglacial sediment thickness around the borehole, from analysis of lag times in VSP data.

Figure 3. A cryoseismic event recorded in the passive DAS acquisition, shown as a) time-space domain, labelling (i) S-, (ii) P-wave arrivals and (iii) S-wave surface reflections, and b) frequency-wavenumber (f-k) response, and the apparent velocities (m s^{-1}; white annotations) it implies. Meaningful information to reconstruct the event in the time-space domain is captured with fewer samples in the f-k domain.

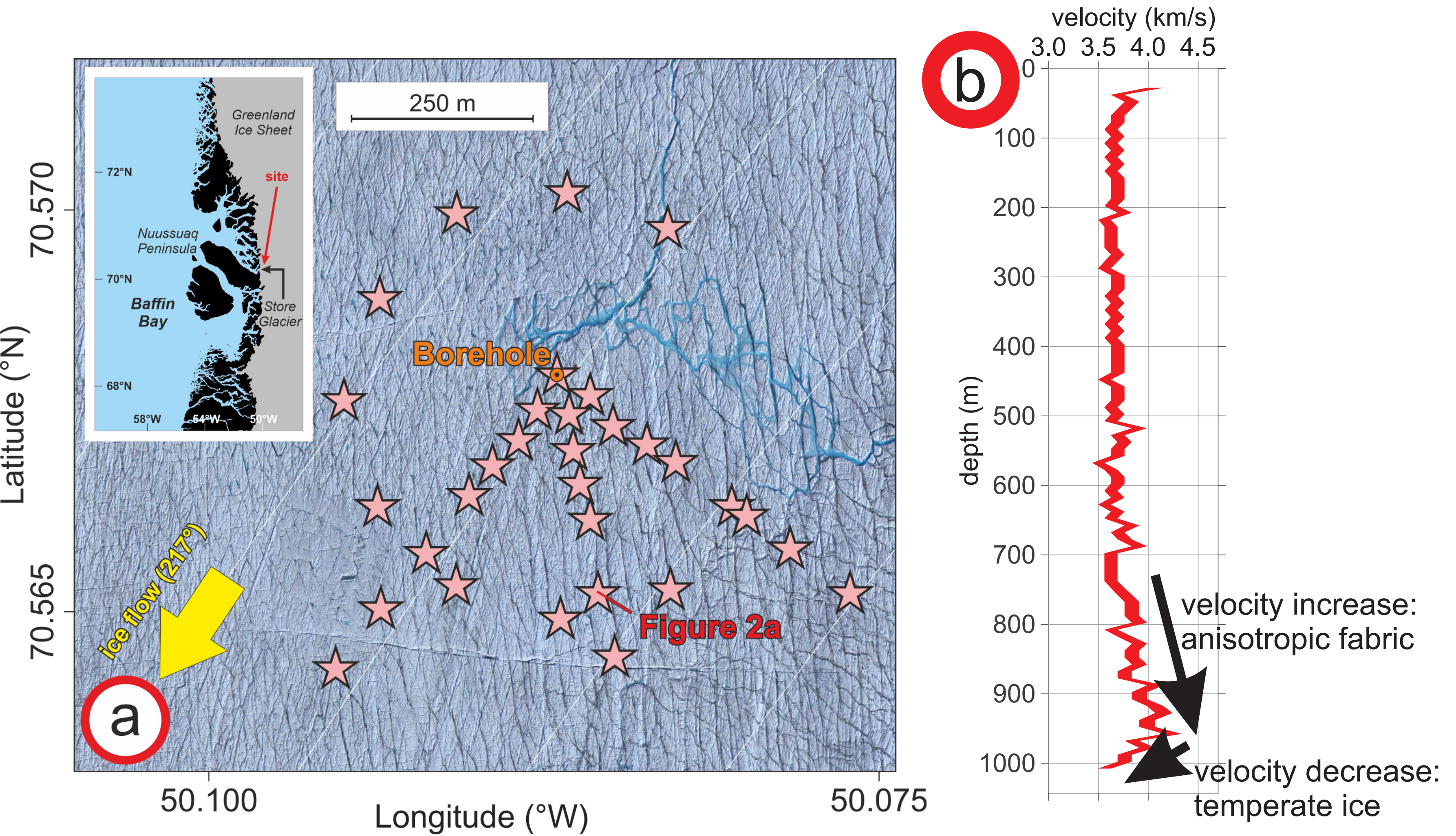

250 m
Greenland
Ice Sheet
site
72°N
70°N
68°N
Nuussuaq
Peninsula
Baffin
Bay
Store
Glacier
58°W
54°W
50°W
Borehole
Figure 2a
ice flow (217°)
a
70.570
70.565
Latitude (°N)
50.100
50.075
Longitude (°W)
b
velocity (km/s)
3.0
3.5
4.0
4.5
depth (m)
0
100
200
300
400
500
600
700
800
900
1000
velocity increase:
anisotropic fabric
velocity decrease:
temperate ice

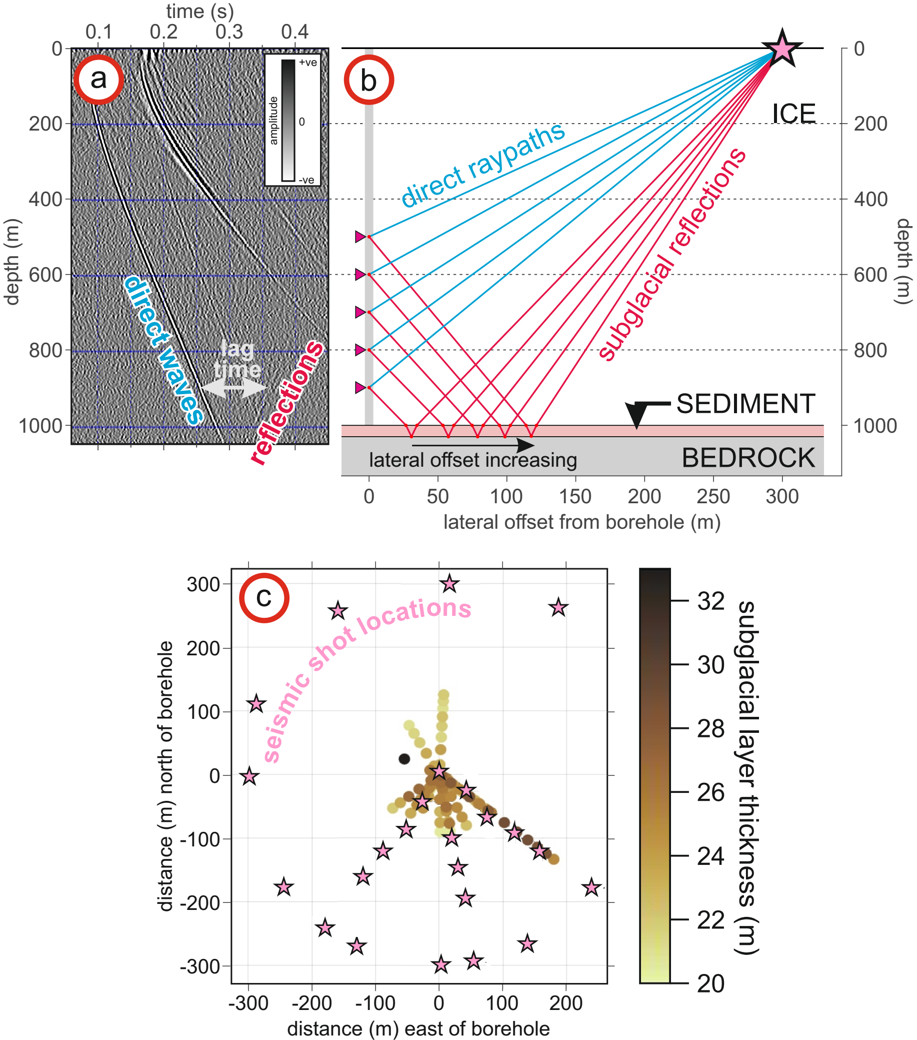

a
time (s)
0.1
0.2
0.3
0.4
depth (m)
0
200
400
600
800
1000
amplitude
+ve
0
-ve
direct waves
lag time
reflections
b
ICE
direct raypaths
subglacial reflections
SEDIMENT
BEDROCK
lateral offset increasing
lateral offset from borehole (m)
0
50
100
150
200
250
300
depth (m)
c
seismic shot locations
distance (m) north of borehole
distance (m) east of borehole
-300
-200
-100
0
100
200
300
subglacial layer thickness (m)
20
22
24
26
28
30
32

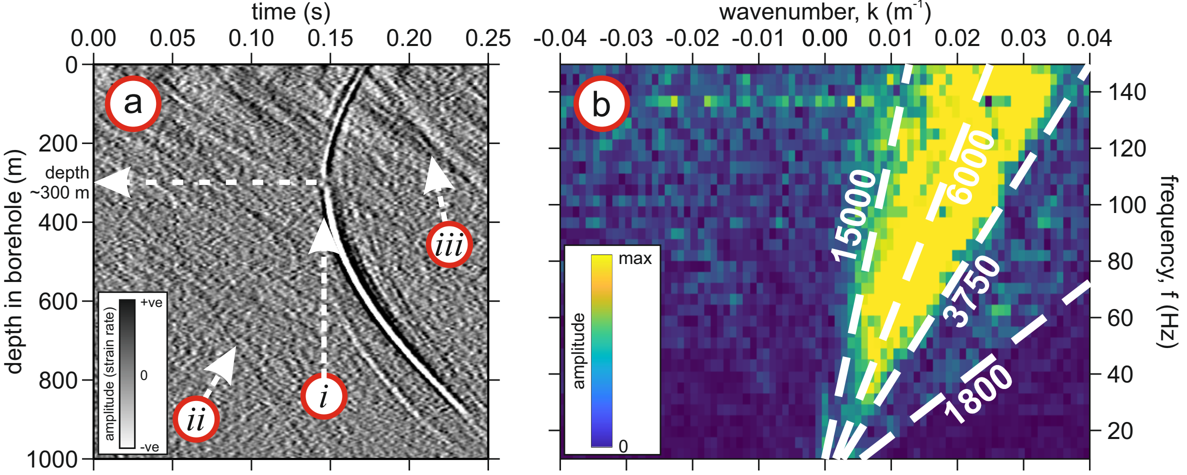

1000 x 1000 data samples

88 x 40 data samples